International Journal of Thermodynamics (IJoT)
ISSN 1301-9724 / e-ISSN 2146-1511
https://dergipark.org.tr/en/pub/ijot

Vol. 27 (No. 2), pp. 059-074, 2024
doi: 10.5541/ijot.1380710
Published online: June 1, 2024

Research Article

Validation of Bluff-body Swirling Flame with RANS Turbulent Model and Comparison of the Results with LES Turbulent Model

[1]O. V. Kazancı, [2]Y. E. Böke

[1]İstanbul Technical University, Mechanical Eng. Faculty, Mechanical Engineering Division 34437, İstanbul, Türkiye.
[2]İstanbul Technical University, Mechanical Eng. Faculty, Mechanical Engineering Division 34437, İstanbul, Türkiye.
E-mail: [1]*kazanci@itu.edu.tr

Recieved 25 October 2023, Revised 20 February 2024, Accepted 29 March 2024

Abstract

The energy required for technological advancement is primarily derived from hydrocarbon combustion, which is a key topic in thermodynamics. The stability of the flame in hydrocarbon combustion is a critical parameter that impacts both burner design and combustion efficiency. Various methods have been employed in the literature to achieve a stable flame, with swirl flow being one technique that enhances combustion performance in engineering applications. This study focuses on the numerical analysis of the SM1 flame from Sydney swirl flames. Initially, the flow incorporating the two-equation Re-Normalization Group (RNG) k-ε and Shear Stress Transport (SST) k-ω turbulence models, along with the chemical reactions of CH_4 combustion using the GRI 3.0 reaction mechanism, was modeled and compared with experimental data. Subsequently, the numerical results obtained from the Shear Stress Transport k-ω turbulence model, which demonstrated the best agreement with experimental data, were compared with results from a numerical analysis in the literature using the Large Eddy Simulation (LES) turbulence model. The predictive capabilities of these two turbulence models, along with their behavior in the flow region, were evaluated. The comparison revealed that for stable flames within the Sydney swirl flame family, the Shear Stress Transport k-ω turbulence model, which provides results in a more efficient manner, is sufficient compared to the computationally expensive Large Eddy Simulation turbulence model. This choice is made possible by utilizing a solution algorithm tailored to the flow characteristics and appropriate boundary conditions.

Keywords: *Swirling flow; thermodynamics; non-premixed combustion; Reynolds Averaged Navier-Stokes; Large Eddy Simulation.*

1. Introduction

Nowadays, the problem of environmental pollution caused by the combustion of fossil fuels demands significant attention. In recent years, the focus has shifted towards finding effective solutions to increase combustion efficiency and reduce emissions [1]. To address this issue, researchers are exploring various combustion methods that can ensure efficient fuel utilization, such as non-premixed turbulent flames involving introducing a swirl into the flow to stabilize the flames. The current emphasis on environmental pollution caused by fossil fuel combustion has led researchers to prioritize improving combustion efficiency and pollutant removal. In understanding this complex relationship, previous studies have highlighted the importance of considering thermodynamic properties of gas combustion. The relationship between gas combustion and thermodynamics is a complex one, influenced by a range of factors. Brinkley highlights the importance of understanding the thermodynamic properties of combustion gases in power plant design, with a focus on thermal equilibrium [2]. Sugawara further explores this, discussing the changes in temperature, velocity, and pressure of combustion gas in a combustion chamber, and their relationship with the fuel-air ratio [3]. Lots of researchers delve into the chemical kinetics of combustion to identify the invariance of the adiabatic temperature for certain combustion mixtures. Lee and Guirao add to this by discussing the gas dynamic effects of fast exothermic reactions, emphasizing the interplay between gas dynamics and chemistry in combustion phenomena [4]. These studies collectively underscore the intricate relationship between gas combustion and thermodynamics, shaped by a range of physical and chemical factors.

In non-premixed systems, the air-fuel mixture is provided before the combustion reaction. Efficient mixing and stable combustion over wide operating ranges are essential for the design of a properly functioning combustor. In many non-premixed systems, fuel is injected into the region of high turbulent flow to increase mixing and geometric or aerodynamic flame stabilizer mechanisms are used to ensure flame stability. The bluff body is one of the classic geometric flame stabilizers. The recirculation zone that occurs behind the bluff body in the flow allows the hot combustion products to be carried upwards, thus ensuring re-combustion and flame persistence. In aerodynamic flame stabilizers, recirculation bubbles, often referred to as vortex breakdown bubbles, are created by the circularity of the flow field. In

*Corresponding Author

some combustors, both types of flame stabilizers can be used to improve air-fuel mixing and flame stability. Such flames are used in industrial applications such as gas turbines and furnaces due to their superiority over non-cyclic turbulent flames [5]. The salient features of swirl stable turbulent flames are increased fuel and combustor mixing, flame stability, flame extinction characteristics, and low emission rates [6].

Swirl stabilized flows and flames have been studied in many experimental studies in the literature. TNF workshops are one of the most comprehensive of these experimental studies [7]. The TNF workshops have well-designed experiments for many different non-premixed flame configurations. Simple jet flames, bluff-body stabilized jet flames and swirl stabilized jet flames are some of the flame types studied in these workshops. The bluff-body stabilized jet flames, a sub-topic of the TNF workshop, provide flames suitable for turbulence-chemistry interaction studies such as piloted burners. Bluff-body burners are also quite similar to real-world combustors that are employed in several industrial settings. Because it retains relatively basic and well-defined boundary constraints while incorporating some of the complexity inherent with real-world combustors, this geometry makes an appropriate compromise for use as a model issue. In TNF Workshops, the bluff-body burner was experimentally studied for several test-cases named HM1e, HM1, HM2, HM3, and HM3e. Swirl stabilized burner, another topic of TNF Workshop, constitutes a natural extension of the bluff-body burner, emerging through the incorporation of a 60 mm inner diameter annulus appended to the bluff-body. This annular addition facilitates the introduction of swirled air, which is delivered tangentially through systematically arranged inlets located at the base of the burner. The swirl-stabilized flame configuration is the most complex test case to determine the accuracy of various turbulence and combustion models because it has two recirculation zones in a specific combination of low swirl number and higher primary axial velocity as opposed to bluff-body stabilized flows, which only have one. There is a Sydney swirl flow project subgroup within the TNF workshops swirl stabilized burner flames. In this subgroup, there are two isothermal swirling flow studies (N29S054 and N16S159) and eight reacting swirling flow (SM1, SM2, SMA1, SMA2, SMA3, SMH1, SMH2 and SMH3) studies for three different fuel types. In first group, SM1 and SM2 flames utilize methane as a fuel and have been tested in the same burner. A swirl coefficient of 0.5 has been employed for both flames. The fuel jet velocity for SM2 is significantly higher than that of SM1. The air jet velocity is consistent for both flames. The impact of the elevated fuel jet velocity has been comparatively investigated. In second group, a mixture of methane and air at a ratio of 1:2 was utilized as the fuel in the flames SMA1, SMA2, and SMA3. The swirl coefficient is 0.66 for SMA1 flame and 1.59 for both SMA2 and SMA3 flames. The study investigated the effects of two different air jet velocities for a constant fuel jet velocity and the effects of two different fuel jet velocities for a constant air jet velocity. In last group, the flames SMH1, SMH2, and SMH3 were fueled with a mixture of methane and hydrogen in a 1:1 ratio. The swirl coefficient is 0.32 for SMH1 flame and 0.54 for both SMH2 and SMH3 flames. The study systematically examined the influence of two distinct air jet velocities while maintaining a constant fuel jet velocity, as well as the effects of two different fuel jet velocities under conditions of constant air jet velocity. The results of these experimental studies have been presented to the literature in several studies with in-depth analysis [8, 9].

The configuration of swirl-stabilized flames is one of the most difficult experimental studies to verify with different turbulence and combustion models [10]. Many working groups have been working on the modeling and verification of these isothermal and reacting experimental studies for about 20 years. In these studies, personal numerical codes and commercial package programs have been used [11, 12] and the results have been published [13].

In their study, Rahman et al. tried to capture the critical flow properties of isothermal turbulent flows stabilized by swirling flow. They investigated the effects of the quality of the mesh structure in critical regions, mesh structure, discretization methods, and various turbulence models on the accurate calculation of flow properties [13]. Researchers underscore the crucial role of mesh resolution in accurately capturing a sizable vortex breakdown bubble. The findings show that 3D RANS simulations can be a useful option for industry, offering a more affordable alternative to the computationally demanding LES. Engineers can gain practical guidance on choosing numerical modeling configurations for complex 3D flow issues.

In a study with 2D axisymmetric geometry, Radwan et al. used Standard and Realizable k-ε, Standard k-ω, and Reynolds Stress Model turbulence models to analyze isothermal turbulent flows of Sydney swirl flow project [11]. In particular, the study aimed to calculate the overall flow behavior and compare it with the experimental model. The numerical investigations showed that among the tested RANS models, Standard k-ω demonstrated acceptable performance in predicting the swirling flow features in both low and high swirl level cases. In addition, the study concluded that the tested RANS models, particularly the one with acceptable performance, can be used as a tool to predict the characteristics of swirling flow in combustor configurations similar to the Sydney swirl burner. Also, researchers implied that the numerical simulations and experimental validation conducted in this study can serve as a reference for future studies on unconfined swirl flow, providing a basis for further research and development in this area.

Yang et al. investigated the SM1 flame, with 2D axisymmetric geometry, using customized Standard k-ε and Realizable k-ε turbulence models in ANSYS Fluent [14]. The researchers stated that the customized Standard k-ε turbulence model is more consistent with the experimental results. Similarly, West et al. tried to calculate the mean and fluctuating velocity values in the flow field using DES (Detach Eddy Simulation) based on SST [15]. Swirl-type regeneration burner was investigated by Fu et al. with four different two-equation turbulence models [16]. The researchers emphasized that SST k-ω and Realizable k-ε models give better results in the flow field. Kashir et al. conducted a comparative study using SST k-ω and Realizable k-ε models in a 2D axisymmetric region [6]. They reported that both models give satisfactory results in the flow field, mixing ratios, temperature, and mass fractions of carbon monoxide in agreement with experimental data. Researchers implied that the prediction of temperature and carbon monoxide mass fraction in the flow field can aid in the design of combustion systems with better control over temperature distribution and reduced CO emissions. They also added that the findings of this study can be used to optimize the design and operation of bluff-body stabilized

swirl flames in practical combustion systems, such as gas turbines and industrial burners [6].

For the swirling flow in the near-burner zone, Weber et al. examined the outcomes of the Reynolds stress model (RSM), k−ε, and an algebraic stress model (ASM) [17]. They found that in the burner quarl area, where the inviscid expansion of flow takes place, the k-ε model introduces a significant inaccuracy. Nonetheless, whirling vortices may be well predicted by RSM and ASM models that use the quadratic upstream differencing (QUICK) discretization scheme for convective components. In another study Gupta and Kumar investigated the dynamics of the three-dimensional flow in a cyclone with tangential inlet and tangential exit using particle tracking velocimetry (PTV) and a three-dimensional computational model [18]. They compared the k-ε and RNG k-ε turbulence numerical models for their suitability in studying the dynamics of pure liquid flowing in a cyclone. According to their findings, the traditional k–ε model is not as good at predicting the flow field as the RNG k–ε model. As a result, they observed secondary recirculating flow and the accurate prediction of its characteristics can help in the development of more efficient separation processes in cyclones, which is important for industries that rely on particle separation and filtration [18].

Christo and Dally used several k−ε models to study the turbulent non-premixed methane/hydrogen flame [19]. They noted that the best agreement with experimental data is shown by the standard k−ε model findings combined with the modified dissipation constant. They also implied that accurate modeling of turbulence, combustion, and chemical kinetics is crucial for predicting the performance of jet in hot flames.

Safavi and Amani conducted one of the most recent studies on the Sydney flames [6]. They compared various steady regime and time-dependent turbulence models such as 2D RANS (Reynolds Averaged Navier Stokes) (RNG k-ε, SST k-ω, Transition SST and RSM (Reynolds Stress Model)), LES (Germano's Dynamic SGS (Sub Grid Scale)), 3D hybrid models (based on SST k-ω) SAS (Scale Adaptive Simulation), Realizable k-ε DES and SST k-ω DES. The results are analyzed focusing on the all flow field and vortex breakdown bubble, which is characteristic of swirl stabilized flames.

Lu et al. modeled the SM1 swirling flame using the Standard k-ε turbulence model with modified coefficients, steady diffusion flamelet combustion model, and DO (discrete ordinate) radiation model [20]. As a result of the analyses, they reported that the turbulence model is inadequate in the regions where the shear stress of the flow is dominant, but in general, it captures the experimental results. Wang et al. demonstrated that Large Eddy Simulation (LES) conducted on a grid of moderate density effectively replicates the precessing vortex core structures in unconfined swirl flow, exhibiting accuracy in both reactive and non-reactive conditions [21]. They also concluded that the observation of vortex structures and spiral-type vortices outside the flame front can provide insights into the flow dynamics and flame behavior, which can be utilized in the development of more efficient and stable combustion systems.

Wegner et al. investigated 3D flow patterns in a non-premixed swirl combustor called the TECFLAM project [22]. They compared time-dependent RANS simulation with experimental results and results obtained with the LES turbulence model. The researchers observed that the time-dependent RANS turbulence model models the flow velocity and vortex core frequency with high accuracy. However, they stated that this turbulence model underestimates the amount of energy in the motion of the precessing vortex core compared to the LES turbulence model. Chen et al. investigated the reactive swirl flow in a combustor with Standard k-ε, RNG k-ε, SST k-ω, and LES turbulence models [23]. They reported that the results obtained with the LES turbulence model are much better than the RANS turbulence models for the flow field and scalar quantities. They also added that the best results among the RANS turbulence models were obtained with the SST k-ω turbulence model.

Apart from RANS simulations, there are also studies on Sydney swirling flames in the literature by Malalasekara et al [24], El-Asrag and Menon [25], Hu et al [26], Xu et al [27], Luo et al [28], Yang and Kaer [12] using the LES turbulence model. In these studies, it was observed that the results obtained from the LES turbulence model were in good agreement with the experimental results in the Sydney swirling combustor. However, the LES turbulence model is not a widely preferred method due to its high cost in core hours. The RANS approach, which is shorter in computer time and lower in cost, has been the predominantly preferred technique in CFD studies to date [29].

The literature survey conducted in this study has shown that RANS analyses with 2D axisymmetric geometry cannot adequately capture the primary flow characteristics of Sydney swirling flames. The vortex breakdown bubble and the upper recirculation zone are three-dimensional in nature and 2D geometries cannot adequately resolve the flow physics of these structures. Therefore, three-dimensional geometries are better choices for solving such flows and are more suitable for use in analysis. A limited number of three-dimensional RANS analyses of Sydney swirling flames are available in the literature, but these studies have focused on predicting the velocity behavior in various flow regimes obtained from isothermal experimental results. In this study, unlike other studies in the literature, the three-dimensional velocity and combustion behavior of SM1, a reactive Sydney swirling flame, is evaluated. It is also aimed to develop a numerical model compatible with the experimental results, to reduce computer time and to provide resources for swirl flame studies.

In the first part of this study, the results obtained from the two-equation RANS (RNG k-ε, SST k-ω) turbulence models (RNG k-ε, SST k-ω), which give successful results in solving swirling flow problems in three-dimensional geometry, are compared with experimental data for the SM1 swirling reactive flow from the Sydney swirl flame family. In the second part of the study, the results of the SST k-ω turbulence model, which gives more consistent results with the experimental data, are compared with the results of the LES turbulence model analysis results which is published. RANS analyses were obtained with the ANSYS Fluent 2020 R1 program. The results of the LES turbulence model are taken from the data shared by Malalasekara et al. in their study [24]. In the literature, there is no such study has been encountered comparing the validations with three-dimensional RANS and LES turbulence models for the SM1 flame. The comparison of the analyses shows that the agreement of the two-equation SST k-ω turbulence model with the experimental data is very similar to the results of the LES turbulence model. For the stable flames of the Sydney

swirl flame family, it is concluded that the use of the two-equation SST k-ω turbulence model, which can be obtained in a shorter time instead of the LES turbulence model, which is much more expensive in terms of core hours, is sufficient and provides analysis without spending much resources by using the solution algorithm suitable for the characteristics of the flow and the correct boundary conditions.

2. Experimental Setup

The Sydney swirl burner selected for the analyses has a radius (*D*) 50mm ceramic surface. In the center of the ceramic surface is a 3.6mm diameter fuel inlet. Swirl flow is provided by a 5mm wide annular region around the ceramic surface. The swirl of the airflow in the burner is achieved aerodynamically by air entering at a 15° angle through 3 tangential inlets located below the air inlet. The combustor is located in the center of a 130x130mm wind tunnel that provides secondary flow to have well-defined boundary conditions. A detailed drawing of the combustor can be seen in Fig. 1 [8].

There are four velocities that are important in the flow characteristics of this combustor. These velocities are the axial velocity U_j of the fuel jet, the axial and tangential velocities U_s and W_s of the air coming circularly from the annular cross-section, and the axial velocity U_e of the secondary airflow coming from the wind tunnel. The geometric swirl value, which indicates the intensity of the cyclic motion in the combustion air, is expressed by S_g. This value is directly proportional to the momentum swirl value S ($S=0.9S_g$). In this study, the SM1 flame from the Sydney swirl flame family was verified. Pure CH_4 was used as fuel in the SM1 flame. The velocity values of the SM1 flame are given in Table 1.

Detailed information about the Sydney swirl burner and experimental results can be found in the literature in the publications of the working group [8, 30, 31].

Table 1. Characteristic velocity values for SM1 flame.

Flame	U_s [m/s]	W_s [m/s]	U_j [m/s]	U_e [m/s]	S_g
SM1	38.2	19.1	32.7	20	0.54

3. Numerical Analysis

In this section, the geometry used in the study, the mesh structure created for this geometry, the independence of the mesh structure, and the solution algorithms selected for the numerical analysis of the physical problem are described. The turbulence models RNG k-ε and SST k-ω, which are used to calculate the flow field in the solution phase, are described in detail in the following sections of this chapter. Detailed information on other solution algorithms can be found in the ANSYS Fluent Theory Manual [32], and other references in the literature.

3.1 Geometry, Mesh Structure and Mesh Independency

The dimensions of the three-dimensional flow field used in this study are shown in Fig. 2. The flow field is considered cylindrical. The outer diameter of the cylinder is 146mm and the length from the air and fuel inlets is 300mm. When creating the geometry, the geometry was extended by 35mm in front of the air and fuel inlets to take into account the effect of the 2° angle in the secondary air flow channel. To generate the mesh structure of the three-dimensional geometry, the mesh generation program within the ANSYS Fluent program was used. The mesh structure of the geometry is shown in Fig. 3 and Fig. 4 as isometric and front view. The mesh is denser in the air and fuel inlet area and coarser towards the end of the geometry. The length of the first element in the inlet region is 0.175mm.

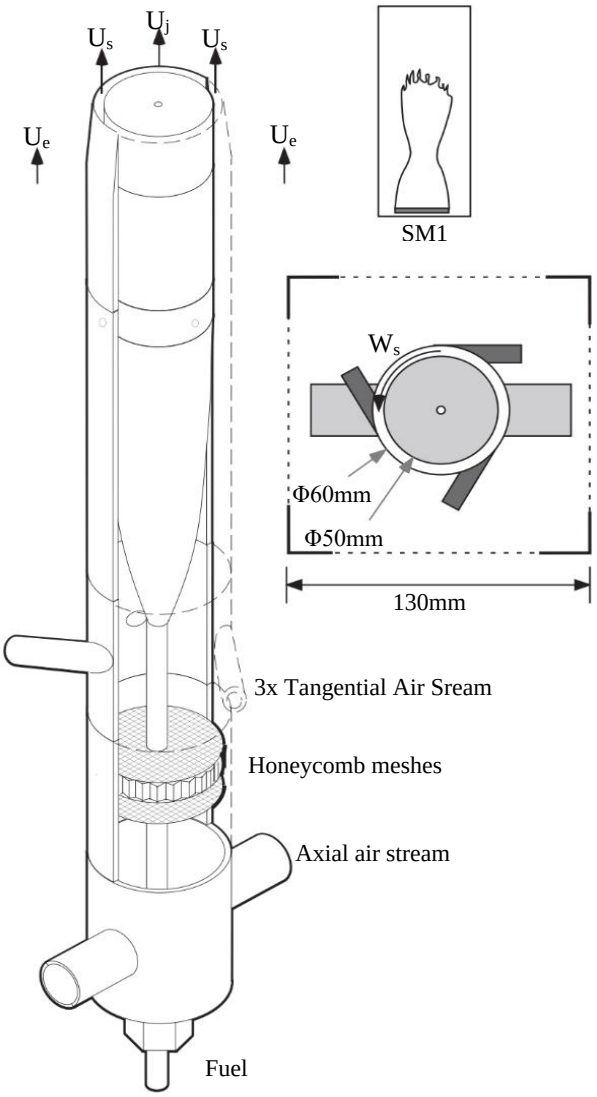

Figure 1. Schematic view of a swirl burner [4].

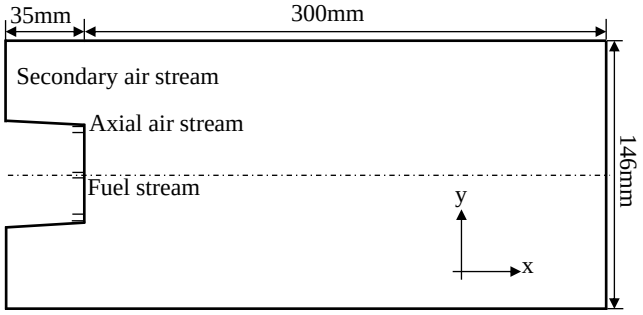

Figure 2. Measurements of three-dimensional geometry.

In order to ensure mesh independency in the analyses, meshes consisting of 2.1M (million), 3.1M and 5.2M structural elements were created. The three mesh structures were numerically analyzed using the SST k-ω turbulence model, appropriate boundary conditions and solution methods. The temperature change in the radial direction in the x/D=1.5 plane is given in Fig. 5. As can be seen from Fig. 5, the difference between the analysis results of the mesh structure with 3.1M elements and the mesh structure with

5.2M elements is quite low. Taking advantage of this result, the mesh structure consisting of 3.1M structural elements was used for all future analyses.

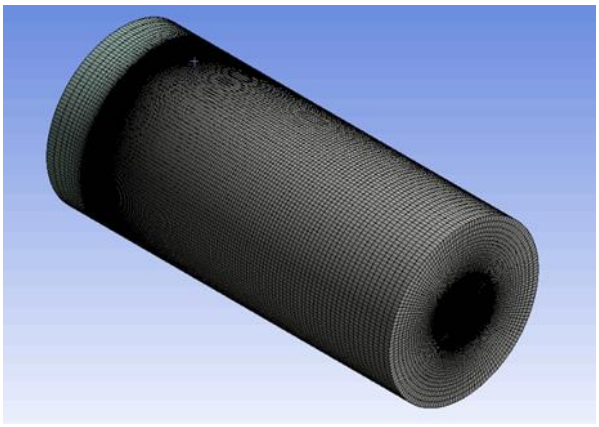

Figure 3. Isometric view of the mesh structure.

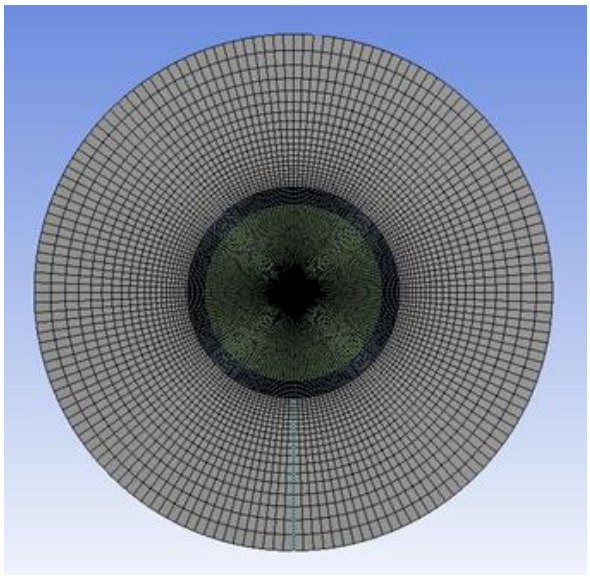

Figure 4. Front view of the mesh structure.

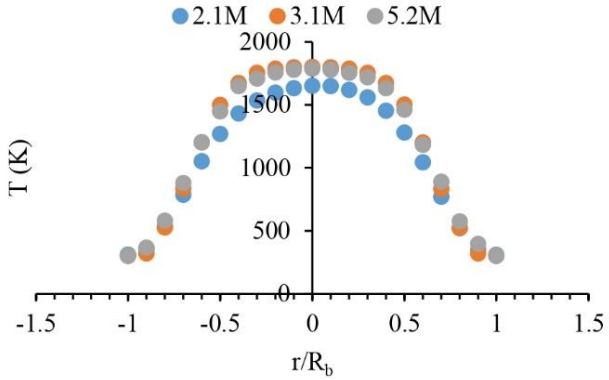

Figure 5. Comparison of temperature values in radial direction for different mesh structures for x/D=1.5.

3.2 Numerical Solution Method

The numerical analysis code of ANSYS Fluent 2020 R1 program was used in the study. RNG k-ε and SST k-ω models were used as turbulence models. P1 was used for radiation and the steady diffusion flamelet sub-model within the non-premixed combustion model was used to model the combustion reaction. The analyses were run in the continuous regime. SIMPLE (Semi Implicit Method for Pressure Linked Equations) model was chosen for the pressure-velocity coupling solution. The PRESTO! method was chosen for pressure calculations, while the QUICK method was chosen for momentum calculations. For other conservation equations and scalar quantities, the second order forward approximation was preferred. The convergence criterion for all equations was taken as 10^{-6}.

3.3 Turbulent Flow Models

The RANS numerical method is a method used in computational fluid mechanics to solve the flow field. They are formed by Reynolds averaging the Navier-Stokes equations. As a result of applying the Reynolds averaging process to the Navier-Stokes equations and organizing these equations, the Reynolds stress term expressed as $-\rho\overline{u_i'u_j'}$ must be solved in order to solve the equations. The most common method used to solve this stress is the Boussinesq approach. Detailed information about this approach can be found in the work of Schmitt F. G. [33]. In order to solve the expression obtained by applying the Boussinesq approximation, the turbulent viscosity μ_t must be solved. After the partial success of the first couplings used for the calculation of turbulent viscosity, it was observed by researchers that this quantity is a property of the flow, not of the fluid, and that convection effects should be taken into account. As a result, methods that take into account convection effects have been proposed. The two-equation RNG k-ε and SST k-ω turbulence models used in this study are among these proposed models.

3.3.1 RNG k-ε turbulence model

The RNG k-ε turbulence model was developed using a statistical method called Renormalization group theory. Compared to the standard k-ε model, the RNG k-ε model takes turbulence fluctuations (eddies) into account and provides an analytical expression for the turbulent Prandtl number. The RNG k-ε model significantly improves the simulation accuracy of the flow by taking into account the effect of large-scale motions, regulating the viscosity governing the operation of small-scale effects, and systematically removing small-scale motions from the control equations. The equations for the quantities k and ε in the RNG k-ε turbulence model are given in Eq. 1 and Eq. 2.

$$\frac{d}{dt}(\rho k)=\frac{\partial}{\partial x_i}\left(\alpha_k\mu_{eff}\frac{\partial k}{\partial x_i}\right)+G_k+G_b-\rho\varepsilon-Y_M \quad (1)$$

$$\frac{d}{dt}(\rho\varepsilon)=\frac{\partial}{\partial x_i}\left(\alpha_\varepsilon\mu_{eff}\frac{\partial \varepsilon}{\partial x_i}\right)+C_{1\varepsilon}\frac{\varepsilon}{k}\left(G_k+C_{3\varepsilon}G_b\right)-C_{2\varepsilon}\rho\frac{\varepsilon^2}{k}-R_\varepsilon \quad (2)$$

In the equations, G_k is the formation of turbulent kinetic energy with respect to mean velocity gradients, G_b is the formation of turbulent kinetic energy with respect to buoyancy, and Y_M is the contribution of the fluctuating dilatation in compressible turbulence to the overall dissipation rate. The expressions α_k and α_ε are the inverse effective Prandtl numbers for k and ε, respectively. The R_ε expression in Eq. 2 is absent in the standard k-ε model and the R_ε expression is as in Eq. 3.

$$R_\varepsilon=\frac{C_\mu\rho\eta^3(1-\eta/\eta_0)\varepsilon^3}{k(1+\beta\eta^3)} \quad (3)$$

$$S_{ij}=\frac{1}{2}\left(\frac{\partial u_i}{\partial x_j}+\frac{\partial u_j}{\partial x_i}\right) \quad (4)$$

In this expression, η is equal to $S(k/\varepsilon)$. The expression for S is equal to $\sqrt{2S_{ij}S_{ij}}$ and the expression for the stress

tensor S_{ij} is given in Eq. 4. Among the constants in these expressions, η_0 has a value of 4.38 and β has a value of 0.012. If the Reynolds number is small and the fluid flow at the wall edge is considered, the turbulence viscosity is calculated as in Eq. 5.

$$d\left(\frac{\rho^2 k}{\sqrt{\varepsilon\mu}}\right)=1{,}72\frac{\hat{v}}{\sqrt{\hat{v}^3\text{-}1\text{-}C_v}}d\hat{v} \quad (5)$$

In this expression, $\hat{v}=\mu_{eff}/\mu$ and C_v is equal to 100. If the Reynolds number is large, the turbulence viscosity is calculated as in Eq. 6. The effective viscosity μ_{eff} is calculated by the formula in Eq. 7. The μ value in Eq. 7 represents the fluid viscosity. The value of C_μ in Eq. 6 is 0.0845.

$$\mu_t=\rho C_\mu\frac{k^2}{\varepsilon} \quad (6)$$

$$\mu_{eff}=\mu+\mu_t \quad (7)$$

The values of the model constants used for the RNG k-ε turbulence model in the ANSYS Fluent program are α_k=1.39, α_ε=1.39, $C_{1\varepsilon}$=1.42 and $C_{2\varepsilon}$=1.68.

3.3.2 SST k-ω turbulence model

The SST k-ω turbulence model is one of the most common models used to observe the effect of turbulence in flow analysis. It is a model with two equations. One equation solves the turbulence kinetic energy (k) term as in the k-ε model, while the other equation solves the specific dissipation rate (ω). The k-ω model has been developed by researchers due to the fact that the solutions with the k-ε model do not give appropriate results, especially in regions close to the wall. First, the standard k-ω model was introduced by David D. Wilcox. Later, the k-ω Base-Line (BSL) model was developed by considering the deficiencies and the SST k-ω model was introduced to the literature by F. R. Menter in 1994. The transport equations and algorithm of the model are explained in the following section of the chapter. Also, the details of the turbulence model can be found in the literature [34].

The SST k-ω model behaves like the k-ε turbulence model in the free flow region, thus eliminating the sensitivity of the standard k-ω turbulence model in the free flow region. The model also provides better flow separation solutions than many other models and takes into account the behavior of inverse pressure gradients. The equations of the model are given in Eq. 8 and Eq. 9.

$$\frac{\partial}{\partial t}(\rho k)+\frac{\partial}{\partial x_i}(\rho k u_i)=\widetilde{P}_k\text{-}\beta^*\rho k\omega + \frac{\partial}{\partial x_i}\left[(\mu+\sigma_k\mu_t)\frac{\partial k}{\partial x_i}\right] \quad (8)$$

$$\frac{\partial}{\partial t}(\rho\omega)+\frac{\partial}{\partial x_i}(\rho\omega u_i)=\alpha\frac{1}{v_t}\widetilde{P}_k\text{-}\beta\rho\omega^2+\frac{\partial}{\partial x_i} \cdot\left[(\mu+\sigma_\omega\mu_t)\frac{\partial\omega}{\partial x_i}\right]+2(1\text{-}F_1)\rho\sigma_{\omega,2}\frac{1}{\omega}\frac{\partial k}{\partial x_i}\frac{\partial\omega}{\partial x_i} \quad (9)$$

In the equations, k is the kinetic energy of turbulence, ω is the specific dissipation rate, ρ is the density, u is the velocity vector and μ is the dynamic viscosity. When calculating the model parameters, the constants in the k-ε and k-ω models are calculated using the blending function using the expression $\theta=F_1\theta_1+(1\text{-}F_1)\theta_2$. The blending function F_1 used here is given in Eq. 10.

$$F_1=\tanh\left\{\left\{\min\left[\max\left(\frac{\sqrt{k}}{\beta^*\omega y},\frac{500\nu}{y^2\omega}\right),\frac{4\rho\sigma_{\omega,2}k}{CD_{k\omega}y^2}\right]\right\}^4\right\} \quad (10)$$

$$CD_{k\omega}=\max\left(2\rho\sigma_{\omega,2}\frac{1}{\omega}\frac{\partial k}{\partial x_i}\frac{\partial\omega}{\partial x_i},10^{-10}\right) \quad (11)$$

The expression for $CD_{k\omega}$ in the expression for the blending function is given in Eq. 11. The y value in these expressions represents the distance from the nearest wall. In the model, μ_t represents the turbulence fluctuation viscosity. The formula for μ_t is given in Eq. 12.

$$\mu_t=\frac{\alpha_1\rho k}{\max(\alpha_1\omega,SF_2)} \quad (12)$$

S in Eq. 12 is equal to $\sqrt{2S_{ij}S_{ij}}$. The F_2 value in this expression is the second blending function of the model. The expression for F_2 can be seen in Eq. 13.

$$F_2=\tanh\left[\left[\max\left(\frac{2\sqrt{k}}{\beta^*\omega y},\frac{500\nu}{y^2\omega}\right)\right]^2\right] \quad (13)$$

$\widetilde{P}_k$ in Eq. 8 and Eq. 9 is the production term. In Eq. 14, the expression $\widetilde{P}_k$ can be seen. In Eq. 13 there is a limit function to prevent the development of turbulence in the separation regions of the flow. The expression for P_k is given in Eq. 15.

$$\widetilde{P}_k=\min(P_k,\,10\cdot\beta^*\rho k\omega) \quad (14)$$

$$P_k=\mu_t\frac{\partial u_i}{\partial x}\left(\frac{\partial u_i}{\partial x_j}+\frac{\partial u_j}{\partial x_i}\right) \quad (15)$$

More detailed information about this model can be obtained from various sources in the literature and ANSYS Fluent Theory Guide [32]. The model constants and values used in the ANSYS Fluent program can be seen in Table 2.

Table 2. Model constants for the SST k-ω turbulence model.

Constant	Value	Constant	Value
$\sigma_{k,1}$	1.176	α^*_∞	1.000
$\sigma_{k,2}$	1.000	α_0	1/9
$\sigma_{\omega,1}$	2.000	β^*_∞	0.090
$\sigma_{\omega,2}$	1.168	R_β	8.000
α_1	0.310	R_k	6.000
$\beta_{i,1}$	0.075	R_ω	2.950
$\beta_{i,2}$	0.0828	μ_{t0}	0.0828
α_∞	0.52	ζ^*	1.500

4. Results and Comparison

This section, where the numerical analysis results are evaluated, consists of two main parts. In the first part, the axial velocity and temperature results of the analyses performed with the two-equation RNG k-ε and SST k-ω turbulence models are compared with the experimental results. In this section, the temperature contours obtained with both turbulence models are also evaluated in terms of the flame shape obtained.

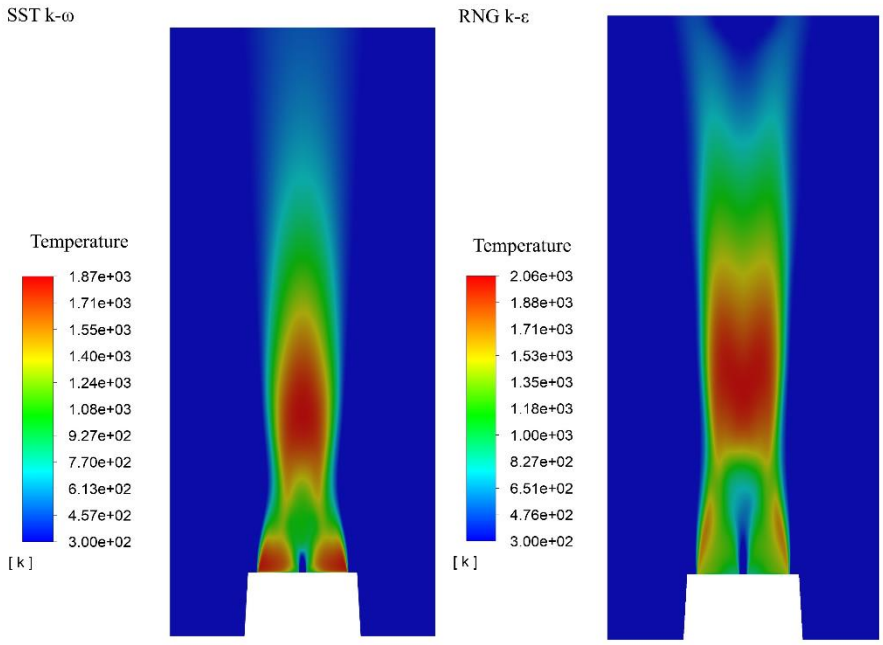

Figure 6. Temperature contours of SST k-ω and RNG k-ε turbulence model solutions.

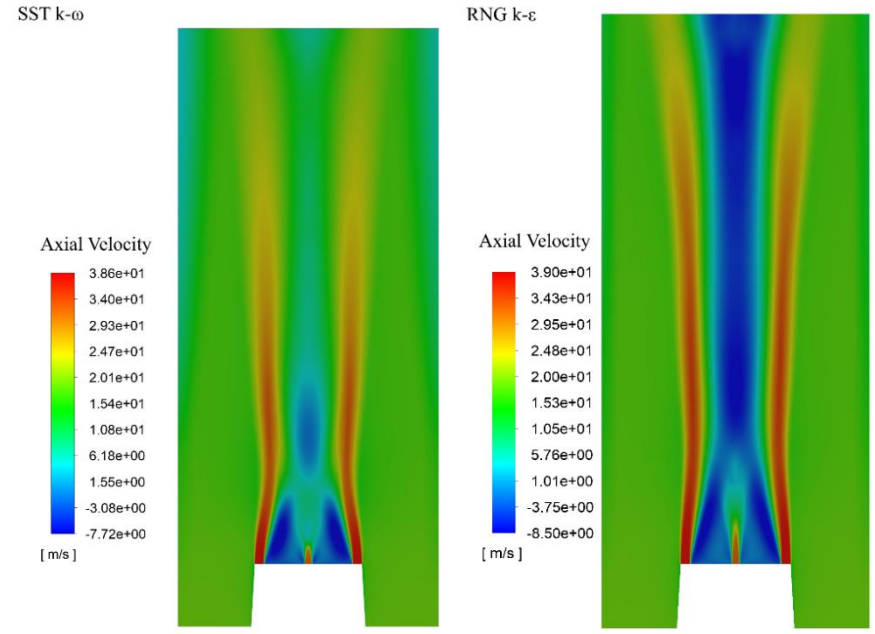

Figure 7. Axial velocity contours of SST k- ω and RNG k-ε turbulence model solutions.

In the second part, the numerical modeling results of axial velocity, tangential velocity, temperature, mean mixture fraction, mass fractions of H_2O, CO and CO_2 components obtained with the SST k-ω and LES turbulence models were compared with the experimental results and the agreement with the experimental results was examined. Pure CH_4 was used as a fuel in all analysis.

4.1 Results for RNG k-ε vs SST k-ω Turbulence Models

Except for the turbulence model, all other solution algorithms are the same. In this section, the temperature contours obtained with the two turbulence models are first analyzed. According to the measurements made by the researchers, the SM1 flame has two flow regions called the first recirculation region and the second recirculation region [8]. The first recirculation zone ends 43mm from the bluff body surface, while the second recirculation zone starts 65mm from the bluff body surface and ends 110mm from the bluff body surface. The recirculation zone is an important characteristic behavior for swirling flames. The flow in these regions is quite complex. Therefore, the first goal of numerical approaches is to accurately calculate these recirculation zones [14]. The recirculation regions of the SM1 flame obtained by numerical analysis of SST k-ω and RNG k-ε are shown in Fig 6.

As can be seen in Fig. 6, the characteristics of the SM1 flame are better predicted by the SST k-ω turbulence model. Both the upper recirculation region and the lower recirculation region resulting from vortex breakdown are more pronounced. The neck region of the flame is also more pronounced than the solution of the RNG k-ε turbulence model. In the solution obtained from the SST k-ω turbulence model, the flame spreads more on the bluff body surface. In the results of the RNG k-ε turbulence model, the flame adheres to the bluff body surface from the outer periphery,

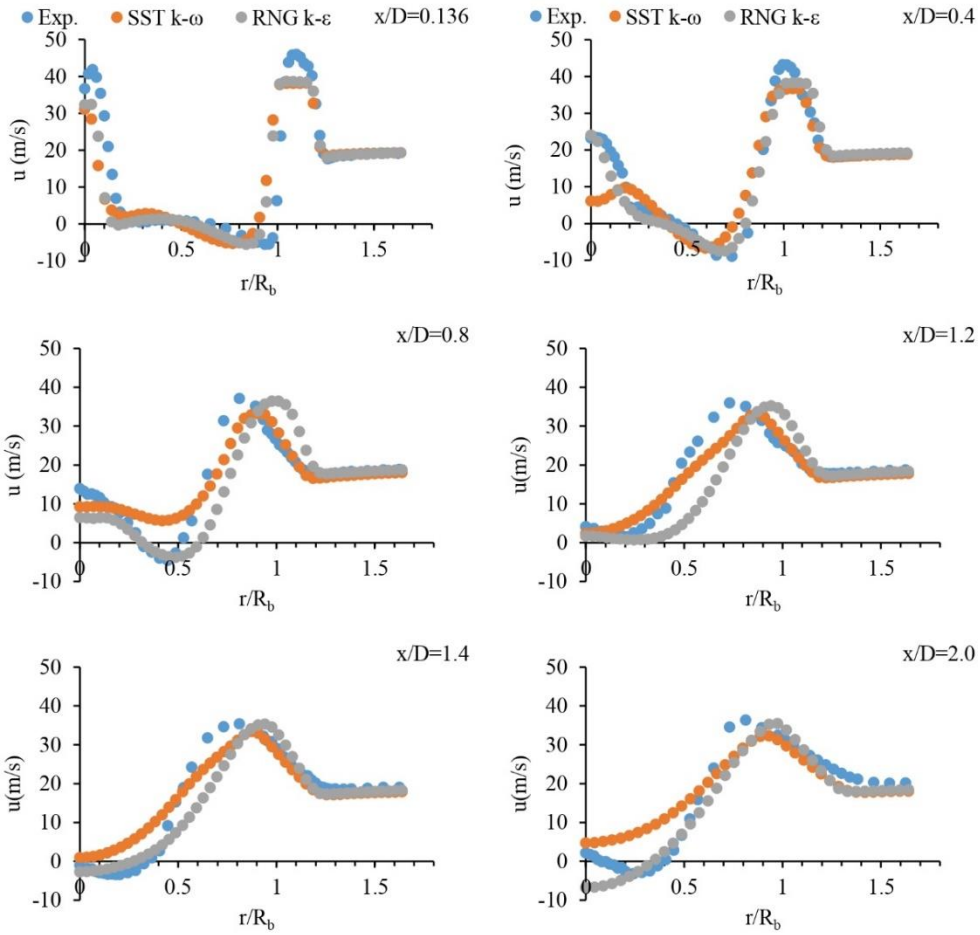

Figure 8. Comparison of axial velocity results of SST k-ω and RNG k-ε turbulence models with experimental data.

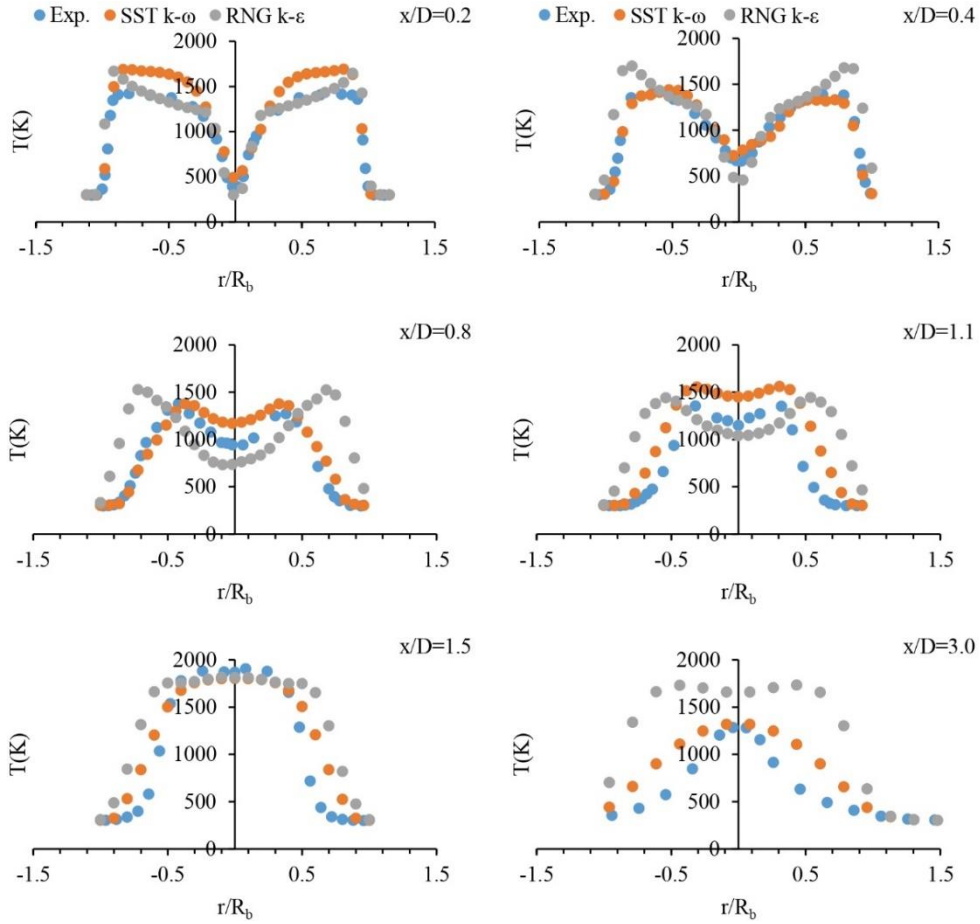

Figure 9. Comparison of temperature results of SST k-ω and RNG k-ε turbulence models with experimental data.

and a colder temperature contour is obtained on the bluff body surface. This is not consistent with the experimentally measured temperature values. In the lower recirculation zone, the results obtained with the SST k-ω turbulence model show that the vortex breakdown bubble is narrower and oval in shape, while the results of the RNG k-ε turbulence model show a wider and rectangular structure. In the comparison for the temperature values obtained from the measurement points in this region, the SST k-ω turbulence model is more consistent with the experimental data.

Axial velocity contours obtained from the numerical solutions of the SST k-ω and RNG k-e turbulence models are presented in Fig. 7. It is noticeable from Fig. 7 that the flame shapes are similar to the velocity profiles. Similar to the temperature contours, the results for the SST k-ω turbulence model show a more pronounced neck of the flame, while the results for the RNG k-ε turbulence model show a higher and thicker neck. In addition, the velocity values show a smaller decrease along the flow domain in the analysis with the RNG k-ε turbulence model. This leads to a longer flame length for the solution of the RNG k-ε turbulence model, which is noticeable in Fig. 6.

The variation of the axial velocities obtained from numerical analysis at different distances upon the bluff body surface is analyzed with the experimental results in Fig. 8. When the diagrams in Fig. 8 are examined, it is seen that the RNG k-ε model gives similar results with the SST k-ω turbulence model in terms of axial velocities and the analysis of both turbulence models for axial velocity values are compatible with the experimental results. At axial distances x/D=0.8 and x/D=1.2, in the range r/R_b=0.6 and r/R_b=1.2 ($R_b = D/2$), it is seen that the RNG k-ε turbulence model fails to capture the experimental results and the velocity profile shifts slightly off-center.

When the temperature data in Fig. 9 are analyzed, the results in the contour plots are better understood. The RNG k-ε turbulence model predicts higher temperatures than the SST k-ω turbulence model, especially in the upper recirculation region, and predicts the temperature values in a narrower region in the radial direction. This is also seen in the RNG k-ε temperature contour in Fig. 6. Except for the axial distances x/D=0.2 and x/D=0.4, the RNG k-ε model calculates the flame wider than the experimental results and the SST k-ω model at all other measurement points, but at the measurement point x/D=3.0, it both calculates the flame wider and overestimates the flame temperatures. The temperature data in Fig. 9 are also consistent with the temperature contours. The fact that the two turbulence models give different results for temperature values when the solution algorithm used in both models is the same suggests that the turbulence-chemistry interaction between the turbulence model and the steady diffusion flamelet model does not behave similarly for each turbulence model. As a result of the numerical analysis, it is concluded that the SST k-ω turbulence model models the SM1 flame better than the RNG k-ε turbulence model. In the second part of the evaluation of the results, the results obtained with the SST k-ω.

4.2. Results for SST k-ω and LES Turbulence Model

The results of the SST k-ω model for the SM1 flame, which are consistent with the experimental data, are compared with the results of the analysis of the SM1 flame with the LES turbulence model code (PUFFIN) developed by Malalasekara et al [24]. The experimental results are also included in all diagrams used for comparison in order to simultaneously see how well the turbulence models match the experimental data. Figure 10 shows the axial velocity data.

As can be seen from Fig. 10, the numerical results show a similar trend with the experimental results. The negative velocity values at the axial points x/D=0.136 and x/D=0.4 within the upward recirculation zone indicate the reverse flow due to the presence of the bluff body surface and are captured by both the SST k-ω and the LES turbulence model. The value of the axial velocity in the x/D=0.4 plane is underestimated by the SST k-ω turbulence model. This is because the SST k-ω turbulence model, which is a RANS turbulence model, has a limited capacity compared to the LES turbulence model in shear stress dominated flows. The recirculation region in the downstream flow due to the presence of vortex breakdown leads to negative axial velocities around the centerline. In this region, both turbulence models can calculate the swirl flow with acceptable accuracy. The data of the SST k-ω and LES turbulence models have a similar orientation with slight differences in the radial direction.

Figure 11 shows the results of the tangential velocity. For the measurement points x/D=0.136 and x/D=0.4, both turbulence models failed to capture the experimental data in the range r/R_b=0.2-1.0. This is due to the shear layer instability in the upper recirculation region and the fuel jet dispersion not being modeled well enough by the turbulence models [24]. In the lower recirculation region starting from the measurement point x/D=1.2, the SST k-ω model shows much more consistent behavior with the experimental results than the previous measurement points. The results of the variation of the tangential velocity of the LES turbulence model are better than the SST k-ω turbulence model for all measurement points.

Figure 12 shows the variations of the mean mixture fraction, f, at different axial distances from the fuel inlet cross section. As can be seen in the diagrams, the results of the SST k-ω and LES turbulence models are similar and show a behavior consistent with the experimental results. In the results of both models, the mean mixture fraction values are lower than the experimental data in the radial range r/R_b=0.4-0.8, especially in the regions close to the bluff body surface such as x/D=0.2 and x/D=0.4. This is due to the fact that turbulence models cannot calculate the propagation of the fuel jet due to tangential velocity well enough and model the flow of the fuel jet as straight. The mean mixture fraction values calculated lower than the experimental data were close to the stoichiometric mixing values. The stoichiometric mixing ratio is indicative of the flame front and is the ratio at which the calculated flame temperatures reach the highest value. For this reason, in areas where the mean mixture fraction is low, the flame temperature is higher than the experimental results. This is also seen in the temperature distribution diagram in Fig. 13. It can be observed from the diagrams that the SST k-ω model obtains lower values than the experimental results, especially near the centerline, at the x/D=0.8 and x/D=1.1 axial measurement points corresponding to the neck region of the SM1 flame. In these regions, the LES turbulence model shows more consistent behavior with the experimental data.

In the lower recirculation zone, the SST k-ω turbulence model predicted the experimental data, especially the

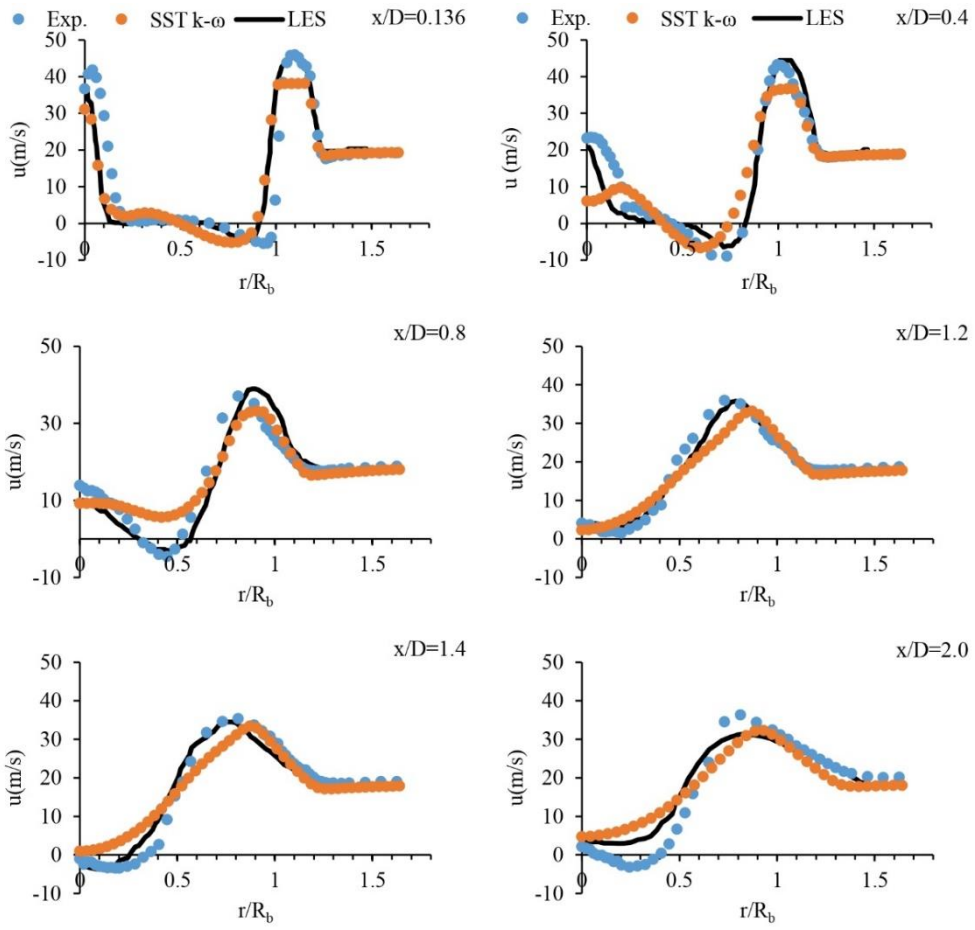

Figure 10. Comparison of axial velocity values of SST k-ω and LES turbulence models with experimental data.

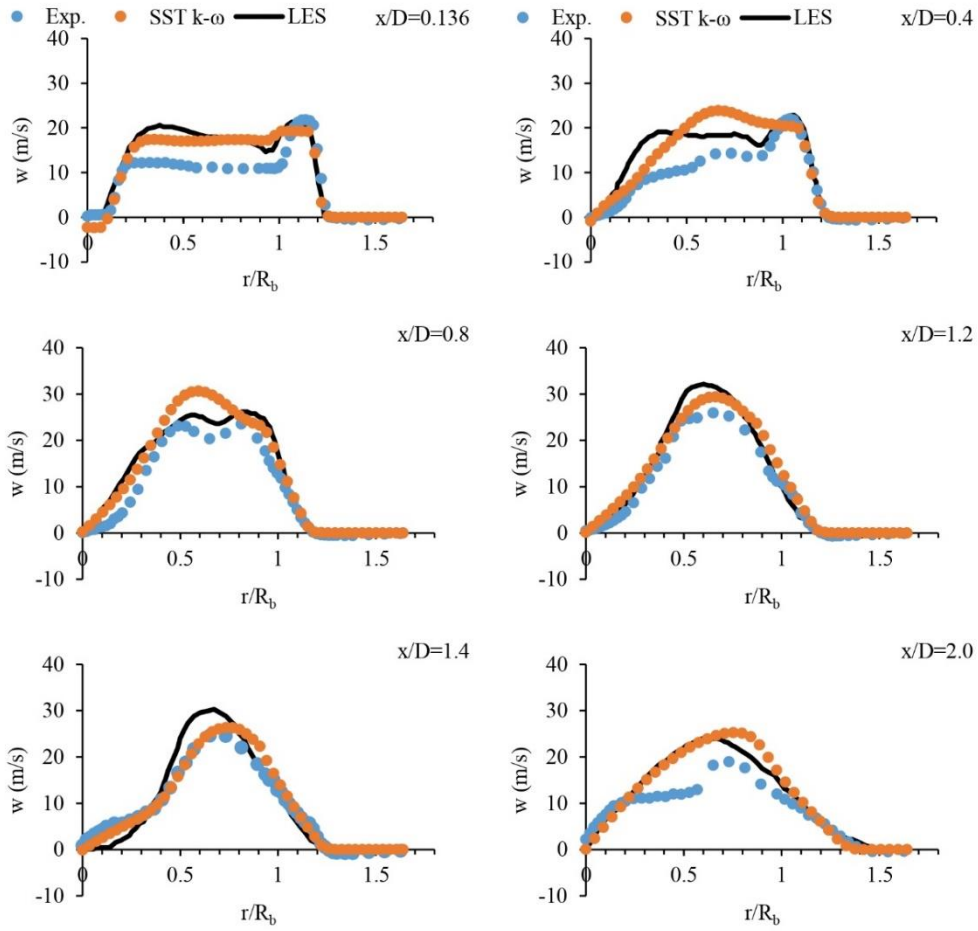

Figure 11. Comparison of tangential velocity values of SST k-ω and LES turbulence models with experimental data.

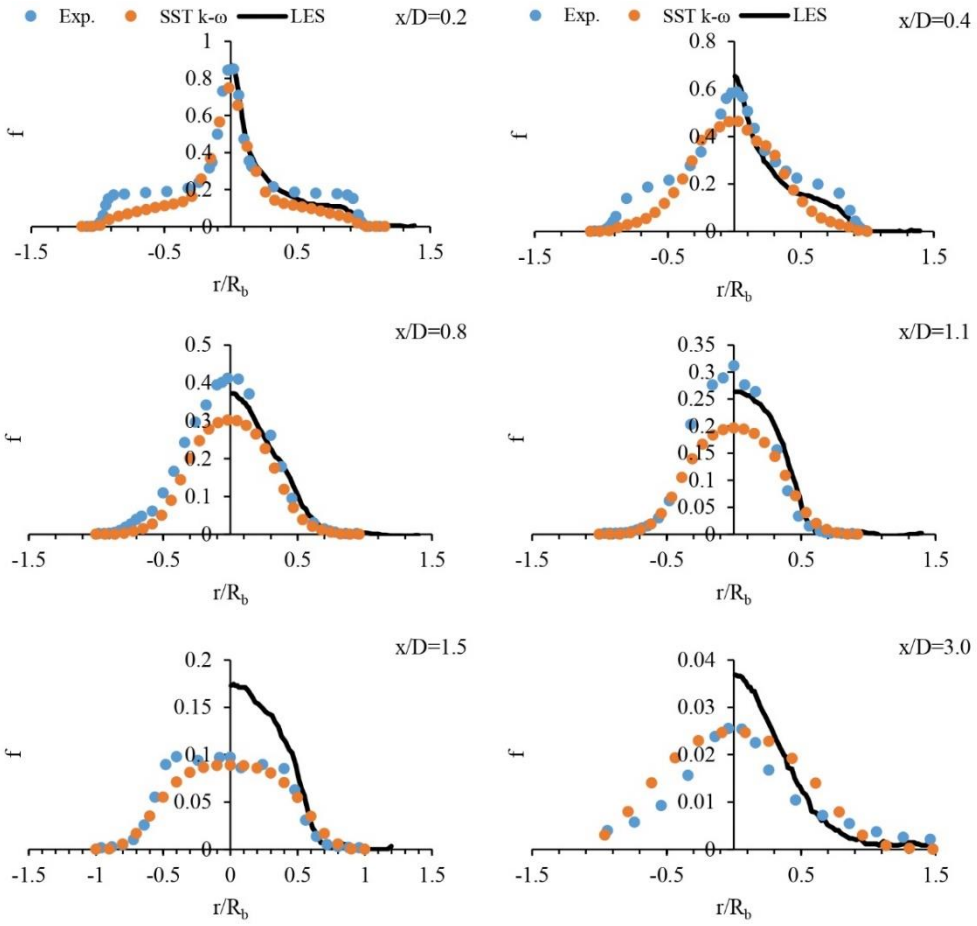

Figure 12. Comparison of mean mixture fraction values of SST k-ω and LES turbulence models with experimental data.

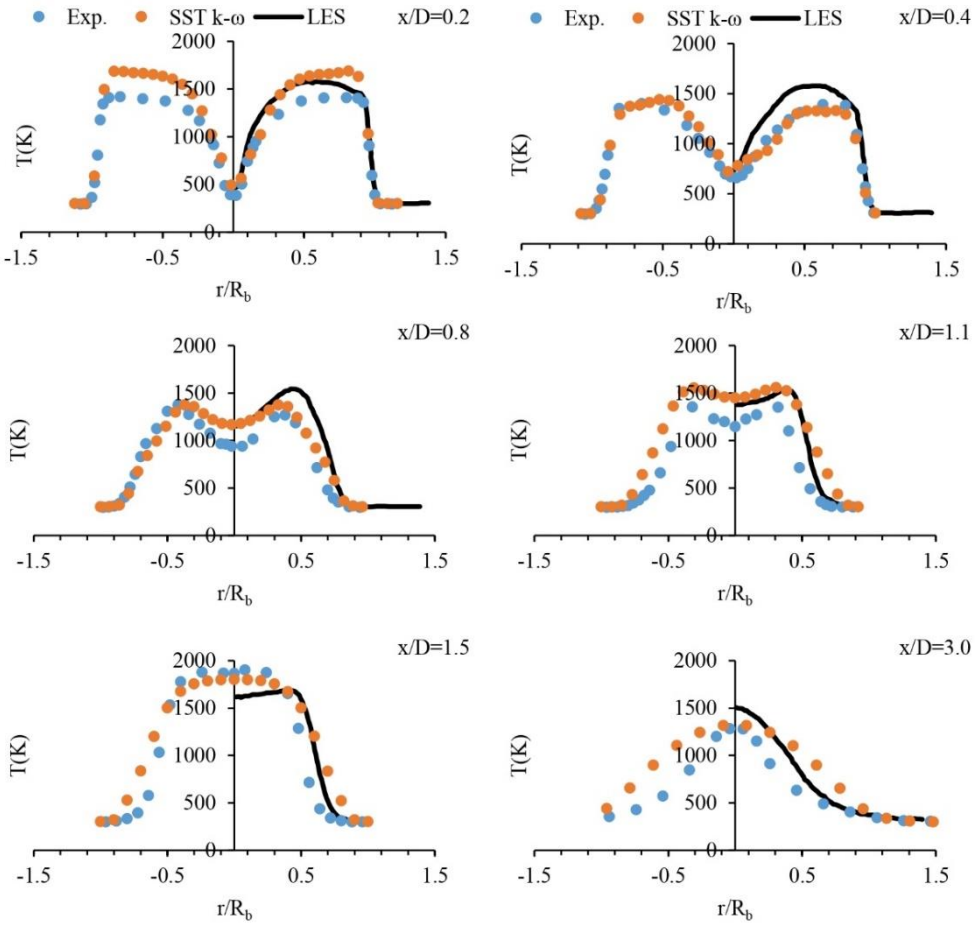

Figure 13. Comparison of temperature values of SST k-ω and LES turbulence models with experimental data.

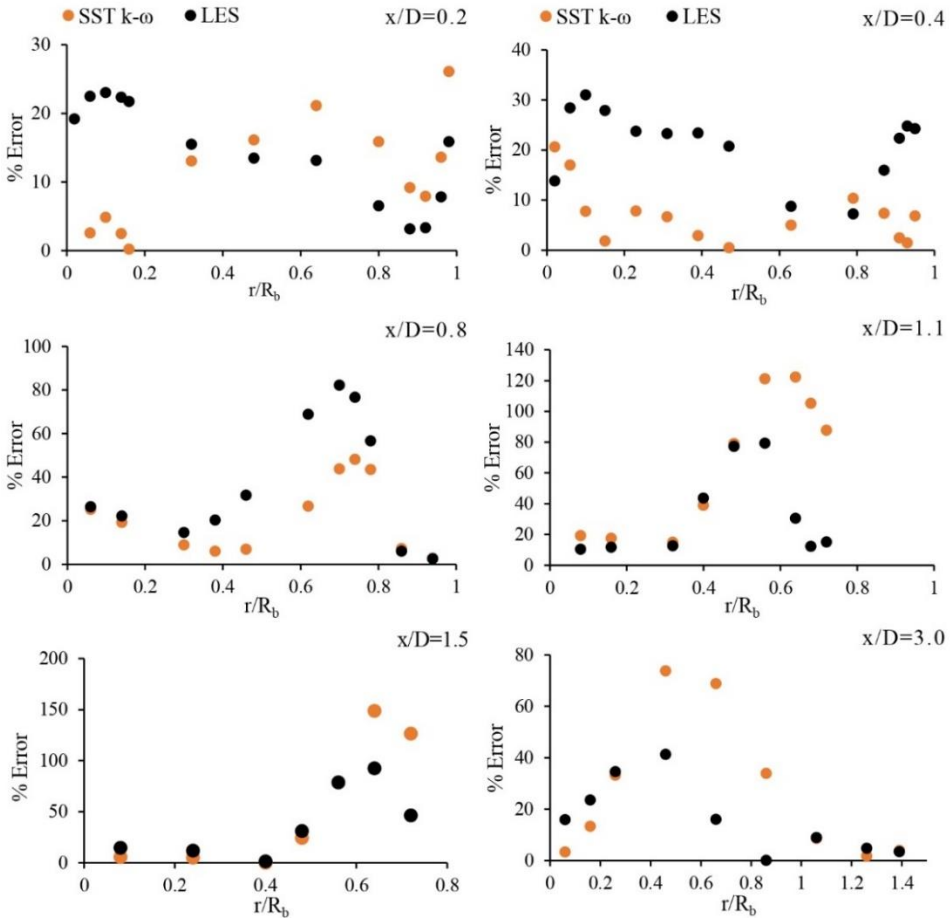

Figure 14. Comparison of %Error values of temperatures of SST k-w LES.

maximum temperature values, much better than the LES turbulence model. The temperature values calculated by the LES turbulence model in the lower recirculation zone are also in agreement with the predictions of the mean mixture fraction value shown in Fig. 12 for this zone, and there are deviations from the experimental measurements in the maximum temperature values. Malalasekara et al. attribute this to the fact that the measured region coincides with the stagnation point of the central recirculation zone [24].

Figure 13 shows diagrams comparing the experimental and numerical results of temperature values for different axial points. Considering the complex nature of the flow field and the combustion reaction, the results obtained are quite satisfactory. As mentioned above, in the *x/D* planes close to the fuel inlet plane, the temperature values of the SST k-ω and LES turbulence model analyses are predicted higher than the measured values. In other *x/D* planes, the numerical model and experimental results are consistent. Especially in the lower recirculation region, the SST k-ω model predicted the flame temperatures more accurately in the *x/D*=1.5 and *x/D*=3.0 planes. However, since it overestimates the size of the vortices in the vortex breakdown bubble, the temperature distribution is wider in the radial direction than the experimental results. The results of the analysis with the LES turbulence model agree with the results of the SST k-ω model in the upper recirculation region, while in the lower flow region near the centerline, the temperature values are underestimated for *x/D*=1.5 and overestimated for *x/D*=3.0. The reason for this difference can be seen from the mean mixture fraction diagrams for the LES turbulence model in Fig. 12. Malalasekara et al. attributed the differences in the temperature value in the lower recirculation zone to the high shear stress flows in this region and the inadequacy of the combustion model used. However, it was emphasized that the numerical results are in the same direction as the experimental temperature data [24]. The temperature data from the LES turbulence model, which effectively models the velocity field throughout the entire flow region in accordance with experimental data, deviates from the temperature data predicted by the SST k-ω turbulence model. This discrepancy may stem from the combustion model code used in the analyses by Malalasekara et al. [24], which could exhibit less efficiency compared to the combustion model.

Figure 14 shows the variations of the temperature % error values of the numerical results obtained with the SST k-ω and LES turbulence models in the radial direction for different measurement points. The situation observed in Fig. 12 and Fig. 13 is also seen in Fig. 14. Both models calculate the temperatures with sufficient accuracy, especially in the upper recirculation zone. When examining the radial distributions of errors in the lower recirculation region, it is observed that the numerical results predict a wider flame than actual. Particularly, the high temperatures calculated within the range of r/R_b=0.5 to r/R_b=1.0 for measurement points between *x/D*=0.8 and *x/D*=3.0 lead to high error percentages. This may be due to the inability of turbulence models to capture the chaotic flow in the lower recirculation region or to errors in the calculation of reactions due to turbulence-chemistry interaction. The results, which are sufficient for validation purposes, can be analyzed with different turbulence-chemistry interaction models for further investigation.

Between Fig. 15 and Fig. 17, the mass ratios of H_2O, CO_2 and CO components are compared with the experimental results. As can be seen in the diagrams for the H_2O

component in Fig. 15, the theoretical results have similar trends with the experimental data. The results of the SST k-ω turbulence model generally overestimated the mass fraction value of H_2O, especially in the centerline region. At the measurement point *x/D*=1.5, very close results were obtained. The LES turbulence model, similar to the SST k-ω turbulence model, gave results close to the experimental data and predicted high and low results at some of the H_2O measurement points. The variations in the mass fraction of generally have similar maximum values and radial variations to the temperature distribution.

As the mass fraction variations of CO_2 in Fig. 16 are analyzed, the agreement of the SST k-ω model with the experimental data is very good in the upper recirculation region and in the neck region of the flame, except for the *x/D*=0.4 plane. In the lower recirculation region the results are slightly higher than the experimental data, but the overall prediction of the numerical results is good. It was reported by Malalasekara et al. that the results of the analysis with the LES turbulence model are slightly underestimated in the first two *x/D* planes and significantly underestimated in the *x/D*=1.5 plane. They also emphasized that this behavior is consistent with the temperature and the mean mixture fraction values [24].

Figure 17 compares the mass fractions of CO. The profile of CO mass fraction changes shows a similar trend and similar maximum values as the temperature profile in the *x/D* planes close to the bluff body surface. The CO profile obtained with the SST k-ω turbulence model shows lower values than the experimental results in the *x/D* planes close to the bluff body surface. The values associated with CO are close to the mixture's lean flammability limit. This situation leads to the predicted values of CO being lower than the experimental data within the upper recirculation region. In the lower recirculation part of the flow, this situation improves and the numerical results show a similar behavior to the experimental results like temperature curves. The results obtained with the LES turbulence model show a similar behavior. However, especially in the lower recirculation zone where vortex breakdown occurs, a high mass fraction of CO has been estimated for the measurement point at *x/D*=3.0.

5. Conclusion

In this study, the experimental results of the non-premixed swirl flame SM1 from the Sydney swirl flame family, which is characterized by globally open and stable boundary conditions, were numerically modeled.

The proposed models for the swirl flow problem are evaluated by reviewing the studies in the literature. As a result of this evaluation, it was decided to use the two-equation SST k-ω and RNG k-ε models. The numerical analyses are compared with the experimental results and it is observed that the prediction values of the numerical analysis using the SST k-ω turbulence model are more compatible with the experimental data.

In the second stage of the study, the results obtained for the SM1 flame with the LES turbulence model, which has a high accuracy in turbulence modeling, were compared with the results obtained with the SST k-ω turbulence model. In the comparison for different variables, it is observed that the LES turbulence model predicts the experimental results better than the SST k-ω turbulence model, especially for the velocity variables, as expected.

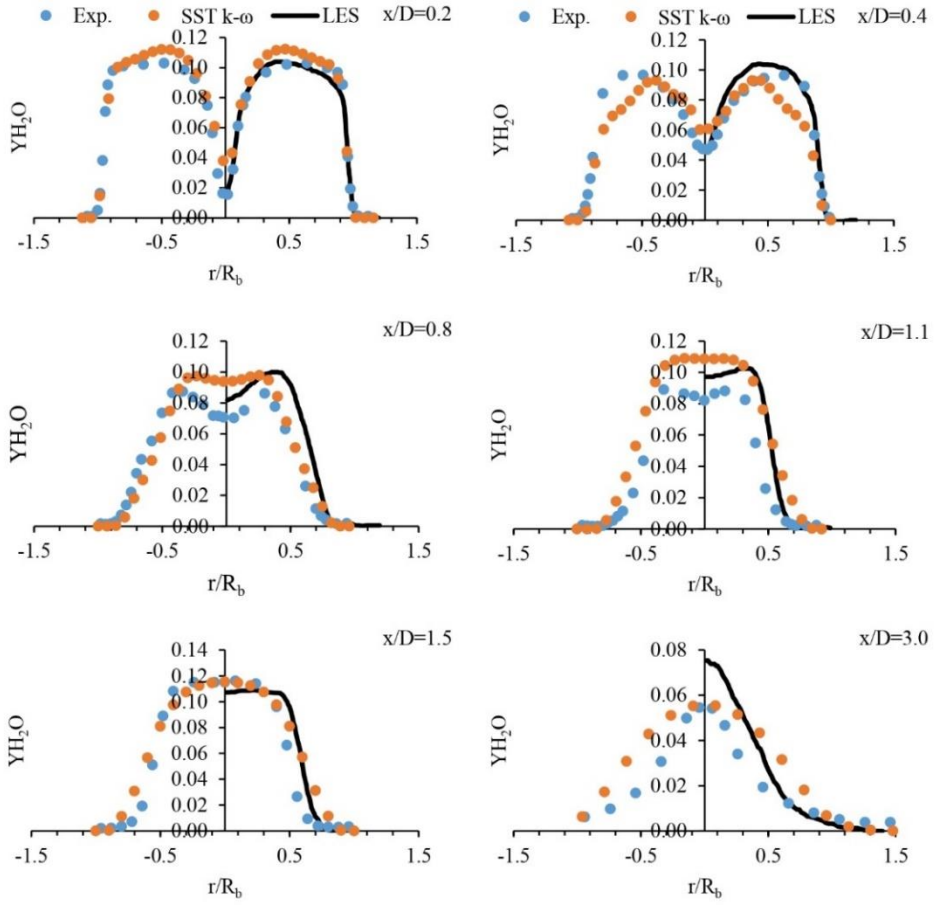

Figure 15. Comparison of H_2O mass fraction values of SST k-ω and LES turbulence models with experimental data.

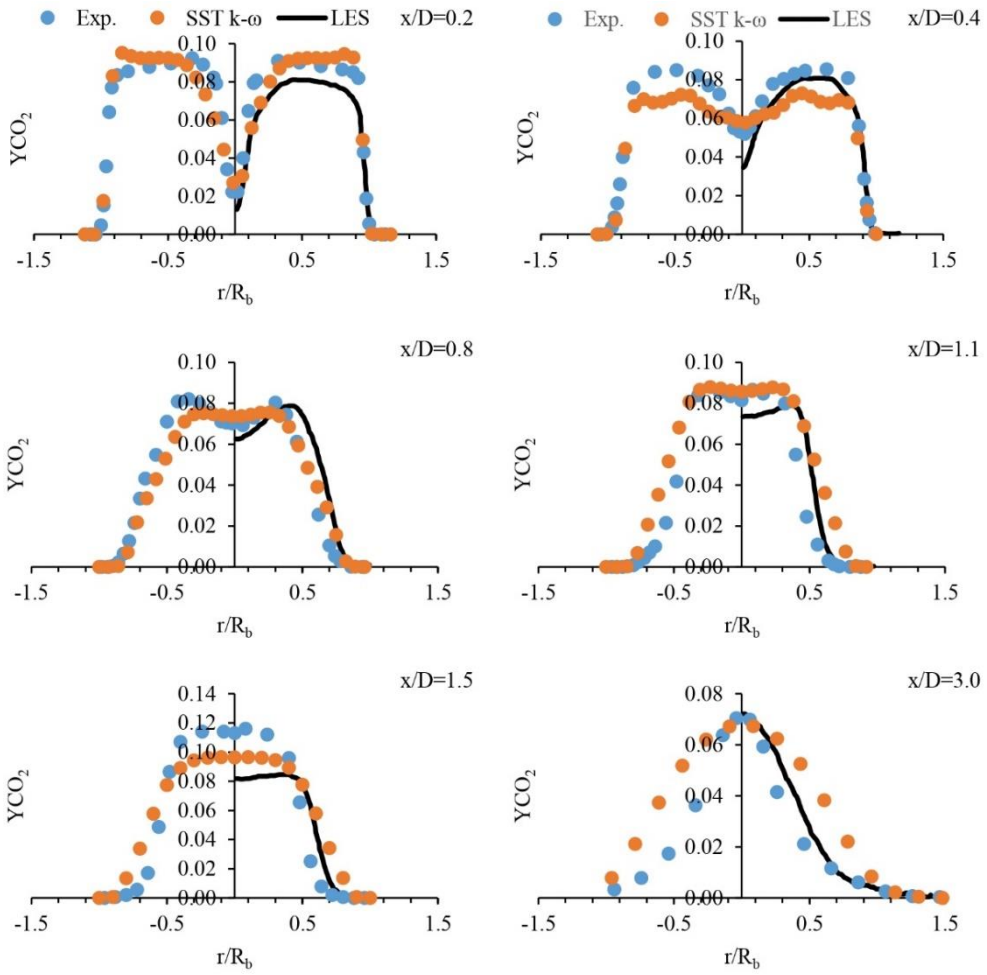

Figure 16. Comparison of CO_2 mass fraction values of SST k-ω and LES turbulence models with experimental data.

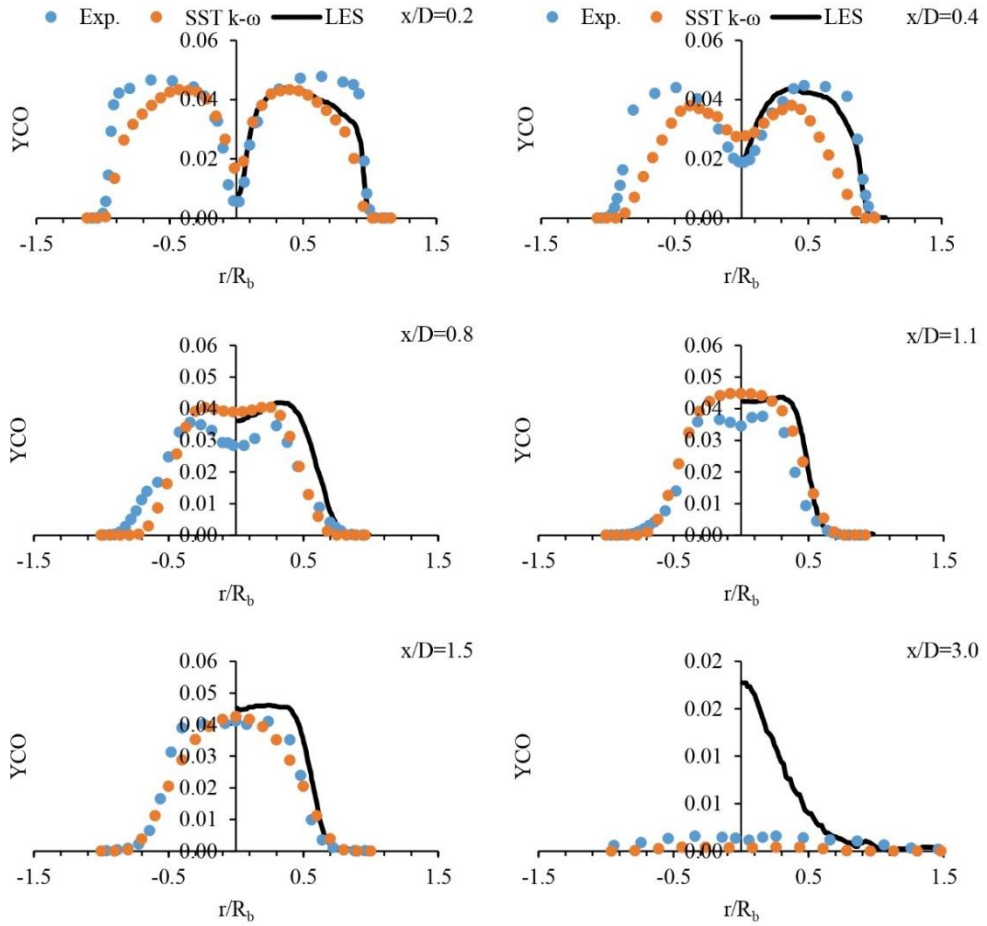

Figure 17. Comparison of CO mass fraction values of SST k-ω and LES turbulence models with experimental data.

When the combustion reaction and the values of the mean mixture fraction, temperature and mass fraction of the components are compared, it is observed that both turbulence models are consistent with the experimental results and even SST k-ω turbulence model gives better results in some x/D planes.

The percentage error values of the calculated temperature values relative to the experimental results have similarly demonstrated that the two turbulence models yield similar solutions in terms of combustion and combustion-related variables. The LES algorithm solves large eddies and models small scales, but combustion occurs structurally at small scales. Therefore, in order to obtain accurate results in modeling combustion reactions, it is possible to make satisfactory predictions without the use of highly advanced numerical techniques such as LES.

By using a geometry that accurately represents the burner, a mesh structure with an ideal distribution, realistic boundary conditions and an accurate solution algorithm, the experimental data of swirl flow flames can be well predicted by the RANS turbulence model. This is also demonstrated in the comparison made in this study. Therefore, RANS turbulence models can be used to model such flames instead of high core-hour cost solution algorithms such as the LES turbulence model, which has a much lower core-hour cost and saves energy and time.

To improve and extend the scope of the study conducted, alternative turbulence-chemistry interaction models will be employed, and their impact on the numerical data will be investigated. Also, exploring the potential of using other alternative fuels or fuel blends in bluff-body stabilized swirl flames to further optimize combustion efficiency and reduce emissions can be done in future.

Nomenclature

α_k	Inverse effective Prandtl number for k
α_ε	Inverse effective Prandtl number for ε
α_0, α_1,α_∞, α^*_∞	Equation constants
β,$\beta_{i,1}$,$\beta_{i,2}$,β^*_∞	Equation constants
$C_{1\varepsilon}$, $C_{2\varepsilon}$, $C_{3\varepsilon}$	Equation constants
C_μ,C_v	Equation constants
D	Diameter of bluff-body (m)
ε	Turbulent dissipation rate (m^2/s^3)
F_1, F_2	Blending functions
G_b	Turbulence kinetic energy with respect to buoyancy(W/m^3)
G_k	Turbulence kinetic energy with respect to mean velocity gradients (W/m^3)
k	Kinetic energy of turbulence (m^2/s^2)
μ	Dynamic viscosity (kg/m·s)
μ_{eff}	Effective viscosity (kg/m·s)
μ_t	Turb. fluctuation viscosity (kg/m·s)
μ_{t0}	Equation constant
ω	Specific dissipation rate (s^{-1})
ρ	Density (kg/m^3)
R_b	Radius of bluff-body (m)
R_β,R_k,R_ω	Equation constants
S_{ij}	Stress tensor
$\sigma_{k,1}$, $\sigma_{k,2}$, $\sigma_{\omega,1}$, $\sigma_{\omega,2}$	Equation constants
u_i, u_j	Velocity component in corresponding direction (m/s)
U_s	Axial air velocity (m/s)
U_j	Fuel jet velocity (m/s)
U_e	Secondary air axial velocity (m/s)
W_s	Tangential air velocity (m/s)
x	Axial distance from fuel inlet (m)
y	Distance from nearest wall (m)
Y_M	Contribution of the fluctuating dilatation in compressible turbulence to the overall dissipation rate (W/m^3)

References:

[1] A. S. M. Al-Obaidi and T. Nguyenhuynh, "Renewable vs. conventional energy: Which wins the race to sustainable development?," *IOP Conf. Ser. Mater. Sci. Eng.*, vol. 434, no. 1, 2018.

[2] S. R. Brinkley Jr., B. Lewis, "The Thermodynamics of Combustion Gase General Considerations" April 1952. https://www.semanticscholar.org/paper/The-Thermodynamics-of-Combustion-Gases%3A-General-Brinkley-Lewis/3f1cbf613422d0b230ab716630acec0b3d34ecd4 (Accessed 22 December 2023).

[3] S. Sugawara and I. Michiyoshi, "The Thermo-Aerodynamical Analysis of Combustion Gas Flow (1st Report)," *Bulletin of JSME*, 1959. https://www.jstage.jst.go.jp/article/jsme1958/2/5/2_5_138/_pdf/-char/en (Accessed 22 December 2023).

[4] J. H. S. Lee and C. Guirao, "Fast Reactions in Energetic Systems," in *Fast Reactions in Energetic Systems*, C. Capellos and R. F. Walker, Eds. NATO Advanced Study Institutes, 1981, pp. 245–313.

[5] B. M. R. De Meester, B. Naud, U. Maas, "Hybrid RANS/PDF Calculations of a Swirling Bluff Body Flame ('SM1'): Influence of the Mixing Model," in *MCS 7*, 2011, vol. 13, no. 1, pp. 43–50.

[6] B. Kashir, S. Tabejamaat, and N. Jalalatian, "A numerical study on combustion characteristics of blended methane-hydrogen bluff-body stabilized swirl diffusion flames," *Int. J. Hydrogen Energy*, vol. 40, no. 18, pp. 6243–6258, 2015.

[7] "TNF Workshop." https://tnfworkshop.org/ (Accessed 22 December 2023).

[8] P. A. M. Kalt, Y. M. Al-Abdeli, A. R. Masri, and R. S. Barlow, "Swirling turbulent non-premixed flames of methane: Flow field and compositional structure," *Proc. Combust. Inst.*, vol. 29, no. 2, pp. 1913–1919, 2002.

[9] A. R. Masri, P. A. M. Kalt, and R. S. Barlow, "The compositional structure of swirl-stabilised turbulent nonpremixed flames," *Combust. Flame*, vol. 137, no. 1–2, pp. 1–37, 2004.

[10] M. Safavi and E. Amani, "A comparative study of turbulence models for non-premixed swirl-stabilized flames," *J. Turbul.*, vol. 19, no. 11, pp. 1017–1050, 2019.

[11] A. Radwan, K. A. Ibrahim, A. Hanafy, and K. M. Saqr, "On rans modeling of unconfined swirl flow," *CFD Lett.*, vol. 6, no. 4, pp. 159–174, 2014.

[12] Y. Yang and S. K. Kær, "Large-eddy simulations of the non-reactive flow in the Sydney swirl burner," *Int. J. Heat Fluid Flow*, vol. 36, pp. 47–57, 2012.

[13] T. M. R. Rahman, W. Asrar, and S. A. Khan, "An investigation of RANS simulations for swirl-stabilized isothermal turbulent flow in a gas turbine burner," *CFD*

Lett., vol. 11, no. 9, pp. 14–31, 2019.

[14] X. Yang, Z. He, S. Dong, and H. Tan, "Combustion Characteristics of Bluff-Body Turbulent Swirling Flames with Coaxial Air Microjet," *Energy and Fuels*, vol. 31, no. 12, pp. 14306–14319, 2017.

[15] J. P. West, C. P. T. Groth, and J. T. C. Hu, "Assessment of hybrid RANS/LES methods for gas-turbine combustor-relevant turbulent flows," *22nd AIAA Comput. Fluid Dyn. Conf.*, no. June, pp. 1–20, 2015.

[16] J. Fu, Y. Tang, J. Li, Y. Ma, W. Chen, and H. Li, "Four kinds of the two-equation turbulence model's research on flow field simulation performance of DPF's porous media and swirl-type regeneration burner," *Appl. Therm. Eng.*, vol. 93, pp. 397–404, 2016.

[17] R. Weber, B. M. Visser, and F. Boysan, "Assessment of turbulence modeling for engineering prediction of swirling vortices in the near burner zone," *Int. J. Heat Fluid Flow*, vol. 11, no. 3, pp. 225–235, 1990.

[18] A. Gupta and R. Kumar, "Three-dimensional turbulent swirling flow in a cylinder: Experiments and computations," *Int. J. Heat Fluid Flow*, vol. 28, no. 2, pp. 249–261, 2007.

[19] F. C. Christo and B. B. Dally, "Modeling turbulent reacting jets issuing into a hot and diluted coflow," *Combust. Flame*, vol. 142, no. 1–2, pp. 117–129, 2005.

[20] M. Lu, Z. Fu, X. Yuan, J. Wu, and S. W. Sabir, "Numerical Simulation of Turbulent Non-premixed Combustion Processes for Methane and Dimethyl Ether Binary Fuels," *ACS Omega*, vol. 6, no. 10, pp. 6629–6642, 2021.

[21] P. Wang, J. Fröhlich, and U. Maas, "Impact of location and flow rate oscillation of the pilot jet on the flow structures in swirling premixed flames," *J. Turbul.*, vol. 11, pp. 1–20, 2010.

[22] B. Wegner, A. Maltsev, C. Schneider, A. Sadiki, A. Dreizler, and J. Janicka, "Assessment of unsteady RANS in predicting swirl flow instability based on LES and experiments," *Int. J. Heat Fluid Flow*, vol. 25, no. 3, pp. 528–536, 2004.

[23] L. Chen and A. F. Ghoniem, "Simulation of oxy-coal combustion in a 100 kW th test facility using RANS and LES: A validation study," *Energy and Fuels*, vol. 26, no. 8, pp. 4783–4798, 2012.

[24] W. Malalasekera, K. K. J. Ranga-Dinesh, S. S. Ibrahim, and A. R. Masri, "LES of recirculation and vortex breakdown in swirling flames," *Combust. Sci. Technol.*, vol. 180, no. 5, pp. 809–832, 2008.

[25] H. El-Asrag and S. Menon, "Large eddy simulation of bluff-body stabilized swirling non-premixed flames," *Proc. Combust. Inst.*, vol. 31 II, no. 2, pp. 1747–1754, 2007.

[26] L. Y. Hu, L. X. Zhou, and Y. H. Luo, "Large-eddy simulation of the Sydney swirling NonPremixed flame and validation of several subgrid-scale models," *Numer. Heat Transf. Part B Fundam.*, vol. 53, no. 1, pp. 39–58, 2008.

[27] J. Xu, D. Huang, R. Chen, and H. Meng, "An Improved NO Prediction Model for Large Eddy Simulation of Turbulent Combustion," *Flow, Turbul. Combust.*, vol. 106, no. 3, pp. 881–899, 2021.

[28] K. Luo, J. Yang, Y. Bai, and J. Fan, "Large eddy simulation of turbulent combustion by a dynamic second-order moment closure model," *Fuel*, vol. 187, pp. 457–467, 2017.

[29] Y. Zhiyin, "Large-eddy simulation: Past, present and the future," *Chinese J. Aeronaut.*, vol. 28, no. 1, pp. 11–24, 2015.

[30] Y. M. Al-Abdeli and A. R. Masri, "Recirculation and flowfield regimes of unconfined non-reacting swirling flows," *Exp. Therm. Fluid Sci.*, vol. 27, no. 5, pp. 655–665, 2003.

[31] Y. M. Al-Abdeli and A. R. Masri, "Stability characteristics and flowfields of turbulent non-premixed swirling flames," *Combust. Theory Model.*, vol. 7, no. 4, pp. 731–766, 2003.

[32] Ansys Inc., "ANSYS FLUENT Theory Guide," *ANSYS Inc., USA*, vol. Release 20, no. R1,http://www.afs.enea.it/project/neptunius/docs/fluent/html/th/main_pre.htm (Accessed 22 December 2023).

[33] F. G. Schmitt, "About Boussinesq's turbulent viscosity hypothesis: historical remarks and a direct evaluation of its validity," *Comptes Rendus - Mec.*, vol. 335, no. 9–10, pp. 617–627, 2007.

[34] Y. Liu, X. Guan, and C. Xu, "An improved scale-adaptive simulation model for massively separated flows," *Int. J. Aerosp. Eng.*, vol. 2018, 2018.